Heat Transfer Coefficients for Fully Developed Internal Flows with Variable Properties and Dissipative Heating

Thomas Drezet[a,*], Peter Ireland[a], Luca di Mare[a]

[a] *Oxford Thermofluids Institute, University of Oxford, Southwell Building, Osney Mead, Oxford, OX2 0ES, United Kingdom*

Abstract

In this paper, numerical simulations of fully developed internal flows are used to disentangle the effects of hydrodynamic and thermal boundary conditions, as well as viscous heating and property variation. Each factor affecting heat transfer is introduced independently to elementary flow simulations, such that 1D analyses may be used to characterise its effects.

Conventional adiabatic wall temperature correlations for accounting for dissipative heating were found to lose their effectiveness when dissipation makes up more than 10% of total heat flux. A more robust method is proposed whereby heat transfer is defined by separate dissipative and convective Stanton numbers. Property variation was found to be well characterised by modified film referencing, with a new formulation proposed which outperforms the classical form. Property variation could also be accounted for by power-laws on temperature ratio, but the results suggest that the exponents are not universal. It was also found that such corrections apply equally to heated and cooled flows when confounding factors are effectively controlled.

Friction and heat transfer results are then generated for more complex flows over a range of temperature gradients, with realistic constitutive relations such that all phenomena occur simultaneously. Without appropriate correction, the results appear highly scattered for both low (due to dissipation) and high (due to property gradients) temperature ratio heat transfer. The methods developed successfully condense these results onto a single unequivocal *Re*-f-*St* characteristic. The isolation of this characteristic from these secondary factors is invaluable for making valid comparisons between variable-property CFD results and experiments.

This investigation focuses on air at moderate temperatures, however the findings may be expected to take on greater significance in high Mach, high Prandtl number, or cryogenic applications.

Keywords: Dissipation, Property Variation, Fully Developed Flow

1. Introduction

Thermal management is a critical area in a number of emerging technologies such as cryogenic cycles, electric propulsion, and geared turbofan engines[1]. The design of such systems relies on accurate estimates of the heat fluxes. At least in a preliminary design setting, these may be obtained from heat transfer coefficient (HTC) correlations extracted from relevant experiments or calculations. HTC correlations are a synthetic representation of the phenomena taking place in the flow and their effect on the near-wall temperature gradient. For convective heat transfer, this gradient is largely determined by the ability of the flow to exchange heat between the bulk of the flow and the fluid in contact with the wall. For a given flow and thermal boundary condition (BC), the temperature field becomes self-similar when normalised to a reference fluid-to-wall temperature difference. This results in a consistent heat flux occurring per degree of temperature difference. This quantity is the HTC.

For heat transfer to be accurately described by a HTC, the flow must be well constrained by its boundary conditions: a common engineering component where such constraint exists is within the long-thin passages in a compact heat exchanger. In this case, the flow reaches a mechanically fully developed state, allowing heat transfer to be well characterised as a function of the sectional geometry, bulk flow conditions, and thermal boundary conditions. It is common practice to make simplifications[2] which allow HTCs for a given section geometry to be represented by a function of sectional Reynolds number[3].

Thermally fully developed flows are approximated in experiments of finite length by imposing particular thermal constraints on walls. Three effects complicate the extraction of *Re*-*St* correlations from such data: heating by frictional dissipation, thermal boundary condition effects, and sectional gradients in fluid properties. Natural choices of experimental conditions often hide these effects. For example, measurability constraints demand a significant flow of heat, which obscures any contribution from frictional heating at lower Mach numbers. However, this same constraint forces experiments to operate a significant wall-fluid temperature difference. Therefore, approximate correction factors must be used to estimate the constant-property correlation from finite heat-flux results[3]. The unreliability of such correction factors diminishes the reliability of heat transfer correlations, particularly when absolute temperatures are low or heat fluxes are high.

Literature on the relation between constant and variable property HTCs is highly inconsistent[4][5][6][7], due to an evidence gap between heating and cooling experiments. This gap

*Corresponding author, email: thomas.drezet@pmb.ox.ac.uk

exists due to practical constraints: firstly, the aforementioned difficulty in measuring small heat fluxes prevents HTC measurement near the constant property limit. Secondly, thermal boundary conditions are not consistent between heating and cooling works, with cooled flow works generally employing water jacket rigs, whereas heated flow works generally opt for electrical heating. The incohesive nature of this experimental body severely limits the certainty by which general conclusions can be drawn[7][8].

In this work, numerical simulations will be used to rigorously characterise the effect of viscous dissipation, thermal boundary conditions, and temperature-dependent property effects upon heat transfer. From this, the efficacy of corrective methods are assessed, resulting in a rigorous methodology for mapping between realistic heat transfer predictions and idealised (I.E. passive temperature) correlations.

Nomenclature

ΔT	Temperature Relative to Wall ($T - T_w$)
$\dot{q}$	Heat Flux to wall per unit area
St	Stanton Number: HTC/($c_p \rho u$)
μ	Molecular Viscosity (dynamic)
μ_T	Eddy Viscosity (dynamic)
ρ	Density
Br_q	Brinkman Number: $\mu u^2/D\dot{q}$ (u=u_b in present work)
c_p	Specific Heat Capacity at Constant Pressure
D_h	Hydraulic Diameter: 4(Area/Perimeter)
f	Friction Factor (wall shear)/$\frac{1}{2}\rho u_b^2$
Nu	Nusselt Number: HTC(D_h/κ) (where κ is conductivity)
Pr	Prandtl Number: $\mu c_p/\kappa$ (where κ is conductivity)
Qr	Convection-Dissipation ratio (see Equation (21))
r	Recovery Factor (see Equation (6))
Re	Reynolds Number: $\rho u D/\mu$
T	Absolute Temperature
u	velocity
x, y, r, z	Coordinates: sectional plane, radial, and streamwise
(D)	Dissipation-Driven, $^{dT}/_{dz} = 0$ Boundary Condition
(H)	Constant Wall Heat Flux Boundary Condition
(T)	Constant Wall Temperature Boundary Condition
BC	Boundary Condition
HTC,h	Heat Transfer Coefficient: $\dot{q}/\Delta T$ where $\Delta T = T_{ref} - T_w$
Shape Factor:	Perimeter^2/Area
$^+$	In wall units
$_0$	Stagnation Quantity
$_f$	Film Quantity
$_{H/T}$	Convective (from (H)/(T) boundary condition)
$_m$	Modified Quantity
$_{aw}$	Adiabatic Wall Quantity
$_b$	Bulk (mass flow) Average Quantity
$_{CP}$	Constant Property Value
$_D$	Dissipative
$_w$	Wall Quantity

2. Background

2.1. HTC Reference Temperatures for Internal Flows

The sectional heat transfer coefficient is defined as

$$h = \frac{\dot{q}}{\Delta T_{ref}} = \frac{\dot{q}}{T_{ref} - T_w} \tag{1}$$

Where T_w is the wall temperature at the section of interest (assumed peripherally uniform in this work). T_{ref} must represent the fluid temperature local to this section. In this work, T_{ref} defined as the *mixed bulk* (or *mixing cup*) temperature:

$$T_b = \frac{\frac{1}{A}\int_A \rho u T \, dA}{\frac{1}{A}\int_A \rho u \, dA} \tag{2}$$

This is a popular choice for internal flows[3] as the streamwise evolution of T_b is easily related to net heat transfer to the fluid.

2.2. Thermal Boundary Conditions

While the concept of a fully developed *velocity* profile is fairly unambiguous for internal flows[2], streamwise temperature derivatives remain finite in any diabatic flow[1][9]. That being said, the temperature field may be become fully developed when normalised to sectional reference temperatures:

$$\frac{d}{dz}\left(\frac{T_w - T}{T_w - T_b}\right) = 0 \tag{3}$$

Analysis by [10], with temperature as a passive scalar, shows this to occur when wall heat flux decays exponentially in the streamwise direction. The upper and lower bounds for this decay correspond to constant wall heat flux (H) and constant wall temperature (T) boundary conditions respectively, illustrated in Figure 1. It is noted by [10] that most fluid-fluid heat exchanger applications fall somewhere between these cases.

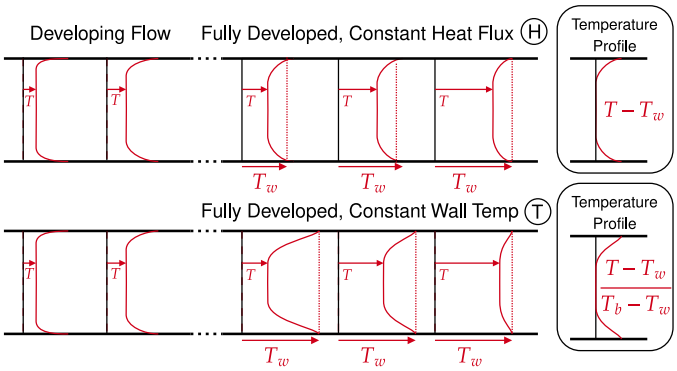

Figure 1: Sketch of fully developed temperature profiles along a pipe

Local streamwise temperature gradient may be derived from condition (3) as:

$$\frac{dT}{dz} = \frac{dT_w}{dz} + \left(\frac{T_w - T}{T_w - T_b}\right)\left(\frac{dT_b}{dz} - \frac{dT_w}{dz}\right) \tag{4}$$

[1] Unless at thermal equilibrium with an internal heat source, e.g. dissipation

For cases (H) and (T), this simplifies to:

$$(\mathrm{H}): \frac{dT}{dz} = \frac{dT_w}{dz} = \frac{dT_b}{dz}, \quad (\mathrm{T}): \frac{dT}{dz} = \frac{T_w - T}{T_w - T_b}\frac{dT_b}{dz}, \frac{dT_w}{dz} = 0 \quad (5)$$

Under the (H) condition, a heated fluid is absorbing heat from a surface at a temperature which linearly increases in the streamwise direction. Experiments [11][12][13] show this to increase the temperature gradient at the wall, thus increase HTC, compared to constant wall temperature (T) boundary conditions. In laminar flows, Nu_H exceeds Nu_T by 9% for channels, but can be higher, e.g. 26% for triangular ducts due to their higher shape factor[2]. In turbulent flows, thermal resistance being concentrated close to the wall results in heat transfer being less sensitive to how temperature gradient is distributed through the flow[2]. Even so, [11] reports Nusselt numbers to be 4.3% higher for the (H) boundary condition than (T) for turbulent boundary layers. Experiments[3] suggest that larger differences may occur for higher sectional shape factors, as temperature gradient distribution for (H) and (T) boundary conditions differs most near the wall. Neglecting such boundary condition effects may mislead experimental findings [8], or introduce uncertainty in CFD validation.

2.3. Dissipation

The temperature distribution in a flow is determined by convection, diffusion, and dissipation. The latter is often neglected[2], however there are engineering flows where this transfer of kinetic to thermal energy is a critical aspect of heat transfer prediction, such as microtube flows (e.g. polymer injection) and high speed flows (e.g. turbomachinery).

Dissipation manifests as an additional source of heat originating within the boundary layer, distorting the temperature distribution and thus affecting HTC. In laminar flow analyses [14][15][16][17], the significance of this effect is quantified by the Brinkman number Br_q, with [18] showing than the introduction of a large degree of dissipation to a fully developed flow (I.E. high Br_q) causes the HTC to more than double. These works also show that dissipation causes a non-zero fluid-wall temperature difference at the adiabatic condition, resulting in a singularity in HTC. Misalignment between ΔT=0 and $\dot{q}$=0 is of particular concern when determining HTCs from finite-velocity duct flows, as it introduces a strong dependence of HTC on wall temperature at small heat fluxes [19]. In high-speed flow works, this is avoided by setting T_{ref} in Equation (1) to the *adiabatic* wall temperature, T_{aw}; I.E. the temperature reached by the wall under adiabatic thermal equilibrium for a flow of given static and total bulk temperature. With this adjustment, heat fluxes may be predicted using HTCs from low speed experiments[2]. In complex turbomachinery flows, experimental [21] and numerical [22] works often evaluate the adiabatic wall temperature field directly, however for simpler flows, adiabatic wall temperature may be estimated in relation to bulk quantities:

$$T_{aw} = T_w + \frac{1}{2} r_b (u^2)_b = T_b + r_b (T_{0b} - T_b) \quad (6)$$

where r_b is the recovery factor; the proportion of dynamic temperature by which the wall exceeds the bulk temperature in the adiabatic case[19][23]. This is particularly convenient as it has been shown in experiments[19][24][25] that this factor is minimally dependent on Reynolds number, with laminar and turbulent flat-plate flows correlating well to $\sqrt{Pr}$ and $\sqrt[3]{Pr}$ respectively[3]. The recovery factors for laminar *internal* flows are significantly different, with pipe flow analysis [26] obtaining a recovery factor equal to Pr. Turbulent pipe flows are seen to behave similarly to external flows due to their flatter velocity/temperature profile, with [19] measuring r_b as 0.88 for turbulent air flow through a pipe, only ~1% different from the corresponding flat plate value.

Universal r_b correlations are usually sufficient for heat flux prediction, however in the present work the zero-flux limit must be approached, thus a greater degree of precision is needed. To achieve this, the principle of superposition[11][27] is used to rigorously isolate the effect of dissipation on the temperature field, including minor geometry and Reynolds number effects. This allows the effect of dissipation on the temperature field to be characterised, and related to the the adiabatic wall-temperature concept for heat transfer prediction.

2.4. Variable Property Effects

Fluid properties vary throughout a cross-section when temperature gradients are significant, causing the flow field to deviate from the constant property solution. This occurs due to property temperature dependence. For example, the viscosity of air increases with temperature[28], resulting in heated laminar flows exhibiting a sharper velocity profile due to viscosity increasing toward the wall[29]. Density also has temperature dependence, decreasing with temperature for ideal gases. Under heating, this results in eddy viscosity increasing away from the wall - in turbulent flows this effect dominates, flattening the velocity profile of heated turbulent flows[30]. Thermal diffusivity, both molecular and turbulent, responds to temperature changes in a similar way to viscosity.

Because gas properties generally scale with some power-law to absolute temperature, it is often proposed to represent the resultant friction factor and Nusselt number variation by a summary power law[3]:

$$\frac{Nu}{Nu_{CP}} = \left(\frac{T_w}{T_b}\right)^n \qquad \frac{f}{f_{CP}} = \left(\frac{T_w}{T_b}\right)^m \quad (7)$$

Popular constants/formulae for n are given in Table 1.

Although correlation[4] is widely accepted[3], Table 1 illustrates a lack of consensus between different experiments. The disappearance of property effects in cooled flows in particular lacks physical basis and evades analytical reproduction[7][6].

[2] In high-speed experiments, dissipative heating invariably causes property variation. Works such as [20] thus attempt to characterise both simultaneously

[3] These investigations apply to external flows, where (6) is based upon free-stream quantities rather than bulk quantities

Source	T_w/T_b	BC	n (in (7))
Humble et al. [4]	1-2.5*	(H)	−0.55
	0.46-.82*	(T)	0
Nicoll et al. [5]	0.33-.66*	(T)	0
Mizushina et al. [6]	0.27-1	(T)	−0.12 - 0
Petukhov [7]	>1	(H)	$-0.36-0.3\ln\left(\frac{T_w}{T_b}\right)$
(semi-analytical)	<1	(H)	−0.36
Fitt et al. [31]	0.3-1.3	(T)	-0.25 ± 0.03

Table 1: Empirical sources for n in (7) for turbulent flows (*average HTCs)

It is proposed by [8][32] that this stems from inconsistency between heating and cooling experiments. In cooled flow experiments, heat transfer is measured when extracting heat from the gas via water jacket, which imposes a (T) BC[4][5][33]. Such experiments calculate HTCs which are averages over a finite length pipe, where wall-fluid temperature difference decays exponentially in the streamwise direction. In heated flow experiments, heat is usually applied electrically[4], producing an (H) BC. These may be expected to capture property effects more accurately as local HTC measurements are made[7], and wall-fluid temperature difference remains more consistent with length under (H) BCs. Fitt et al.[31] is the exception, using transient flat-plate apparatus consistently between heating and cooling tests. While these conditions don't represent fully developed pipe flow, the results do suggest that the distinction between heating and cooling sensitivity seen in other sources may be spurious.

An alternative to (7) used by many works [30][4][33][8] is to modify the definitions of Re and Nu such that results collapse well onto a single line. The modifications consist of evaluating properties at alternative temperatures which better characterise key areas of the flow (e.g. film f, surface s):

Source	Re	Nu
Deissler 1950 [30]	$Re_{mf} = \frac{\rho_f u_b D}{\mu_f}$	$Nu_f = \frac{hD}{\mu_f}$
Humble et al. 1951 [4]	$Re_{ms} = \frac{\rho_s u_b D}{\mu_s}$	$Nu_s = \frac{hD}{\mu_s}$
Sleicher et al. 1975 [33]	$Re_f = \frac{(\rho u)_f D}{\mu_f}$	$Nu_b = \frac{hD}{\mu_b}$

Table 2: Sources redefining Re/Nu to eliminate temperature sensitivity

Here, m denotes a 'modified' quantity whereby ρ is evaluated at the chosen reference temperature while $u_b = \dot{m}/\rho_b A$ is retained.

The works summarised in tables 1&2 show many inconsistencies: while much of this may stem from experimental uncertainty[8], it may also indicate weakness in the common assumption[2] that correction (7) applies consistently between geometries, Reynolds numbers, and boundary conditions.

3. Methodology

The aim of this work is to characterise 3 key thermal effects in terms of their impact on heat transfer correlations for fully developed flow. This is explored by evaluating heat transfer for 3 key flow geometries over a parametric space of Reynolds numbers, temperature ratios, and Mach numbers appropriate to compact heat exchangers[3]:

$$5\times10^3 \le Re \le 2\times10^5, \quad 0.8 \le T_w/T_b \le 1.2, \quad \text{Mach} < 0.1$$

To populate this parametric space at a feasible cost, calculations are performed using RANS methods, which have been carefully optimised such that key DNS/experimental results are accurately reproduced. In sections 4.1-4.3, each feature of interest is characterised individually via 1D computations of pipes and channels, In section 4.4-4.5, the robustness of the proposed characterisations are assessed when applied to 2D computations of a square duct flow with all effects modelled simultaneously.

3.1. 1D Turbulent Computations

1D results are solutions of the momentum and energy equations in terms of streamwise velocity and static temperature:

$$\cancel{\frac{du}{dt}} + u\cancel{\frac{du}{dz}} = \frac{1}{\rho}\frac{dP}{dz} + \frac{1}{\rho}\frac{1}{r^j}\frac{d}{dy}\left(r^j(\mu+\mu_{Tu})\frac{du}{dy}\right) \tag{8}$$

$$\cancel{\frac{dT}{dt}} + \underbrace{u\frac{dT}{dz}}_{\text{convection}} = \underbrace{\frac{1}{\rho}\frac{1}{r^j}\frac{d}{dy}\left(r^j\left(\frac{\mu}{Pr}\frac{dT}{dy} + \overbrace{\frac{\mu_{Tu}}{Pr_t}\frac{dT}{dy}}^{-\overline{v't'}}\right)\right)}_{\text{diffusion}} + \underbrace{\frac{\mu+\mu_{Tu}}{\rho c_p}\left(\frac{du}{dy}\right)^2}_{\text{dissipation}} \tag{9}$$

where setting $j=0$ models a channel while $j=1$ models a pipe.

The solution is obtained via the author's own code as follows: The equations are discretised using a second order, cell centred, finite volume scheme. These are cast as a set of algebraic relations with corresponding analytical derivatives. This system is then solved implicitly by Newton's method. Turbulence is modelled using the non-linear k-ε model of Abe[34], adapted to 1D by defining an equivalent eddy viscosity, μ_{Tu},

$$\mu_{Tu} = \mu_T\left(1 + \frac{11}{3}\left(\frac{C_d\mu_T}{\rho k}\right)^2\left(\frac{du}{dy}\right)^2\right)^{-1}, \quad \mu_T = C_\mu f_\mu \frac{k^2}{\varepsilon} \tag{10}$$

$$\cancel{\frac{dk}{dt}} + u\cancel{\frac{dk}{dz}} = \frac{1}{\rho}\frac{1}{r^j}\frac{d}{dy}\left(r^j\left(\mu + \frac{\mu_T}{\sigma_k}\right)\frac{dk}{dy}\right) + \mu_{Tu}\left(\frac{du}{dy}\right)^2 - \varepsilon \tag{11}$$

$$\cancel{\frac{d\varepsilon}{dt}} + u\cancel{\frac{d\varepsilon}{dz}} = \frac{1}{\rho}\frac{1}{r^j}\frac{d}{dy}\left(r^j\left(\mu + \frac{\mu_T}{\sigma_\varepsilon}\right)\frac{d\varepsilon}{dy}\right) + C_{\varepsilon 1}\mu_{Tu}\left(\frac{du}{dy}\right)^2 - C_{\varepsilon 2}f_\varepsilon\frac{\varepsilon^2}{k} \tag{12}$$

where all model closures are as given in [34]. The contribution of k to Equation (9) is neglected. Turbulent Prandtl number is set locally by Kays's empirical formula[35]:

$$Pr_t = \frac{1}{0.5882 + 0.228\left(\frac{\mu_{Tu}}{\mu}\right) - 0.0441\left(\frac{\mu_{Tu}}{\mu}\right)^2\left[1-\exp\frac{-5.165}{(\mu_{Tu}/\mu)}\right]} \tag{13}$$

μ_{Tu} is used here due to the way Pr_t is defined in [35]:

$$Pr_t = \frac{\overline{u'v'}/du/dy}{\overline{t'v'}/dT/dy} \rightarrow \overline{t'v'} = -\frac{\mu_{Tu}}{Pr_t}\frac{dT}{dy} \tag{14}$$

The grid is set to a height of $\Delta y^+ = 0.7$ at the wall, expanding geometrically up to $\Delta y^+ = 10$. ε is set to $2\nu k/y^2$ in the near-wall cell. The resolution is such that the solution is indistinguishable from a solution obtained using an orthogonal collocation method with spectral accuracy.

The turbulent viscosity and Prandtl number closures have been selected to provide a high degree of accuracy, both thermal *and* mechanical, for the elementary flows examined in this study. This is demonstrated in figures 2a&2b, which show channel and pipe flow predictions to be in excellent agreement with DNS in terms of both friction and heat transfer.

3.2. 2D Turbulent Computations

2D results are computed by a similar method to the 1D results (using the author's own code), now solving the compressible continuity, momentum (x, y, z), energy, k, and ε equations in the sectional plane of a square duct. Convection is modelled by the preconditioned flux of Weiss and Smith[36], and turbulence by the fully anisotropic form of Abe's k-ε model[34]. The turbulent diffusivity defined by (13,14) is retained. The mesh is a simple Cartesian grid with geometric refinement toward the walls. The grid is modified for each Re, ensuring that f and St are independent of grid resolution and that $\Delta y^+ < 0.7$ at the wall.

The flow through a square duct differs from that of a pipe or channel in that the stress and heat flux is not circumferentially uniform. It also includes in-plane convection in the form of secondary flow, shown in Figure 3. Secondary flow predictions are of similar magnitude to DNS, and Figure 4 shows the resulting heat transfer and friction results to be in excellent agreement with DNS and experiment.

3.3. Variable Property Models

Variable density is modelled by the ideal gas law:

$$\rho = \frac{p}{RT} \tag{15}$$

Where p is the local pressure (uniform reference pressure in 1D simulations). Variable viscosity is modelled by Sutherland's law[28]:

$$\mu = \mu_{0c} \frac{T_{0c} + S}{T + S} \left(T/T_{0c}\right)^{1.5} \tag{16}$$

The gas represented is air, with $T_{0c} = 273.15K$, $S = 110.4K$, μ_{0c}=$1.716\times10^{-5} kg/ms$, $R = 287 J/kgK$, $c_p = 1005 J/kgK$, and Pr=0.71. For clarity, ρ and μ are modelled as constant in sections 4.1&4.2.

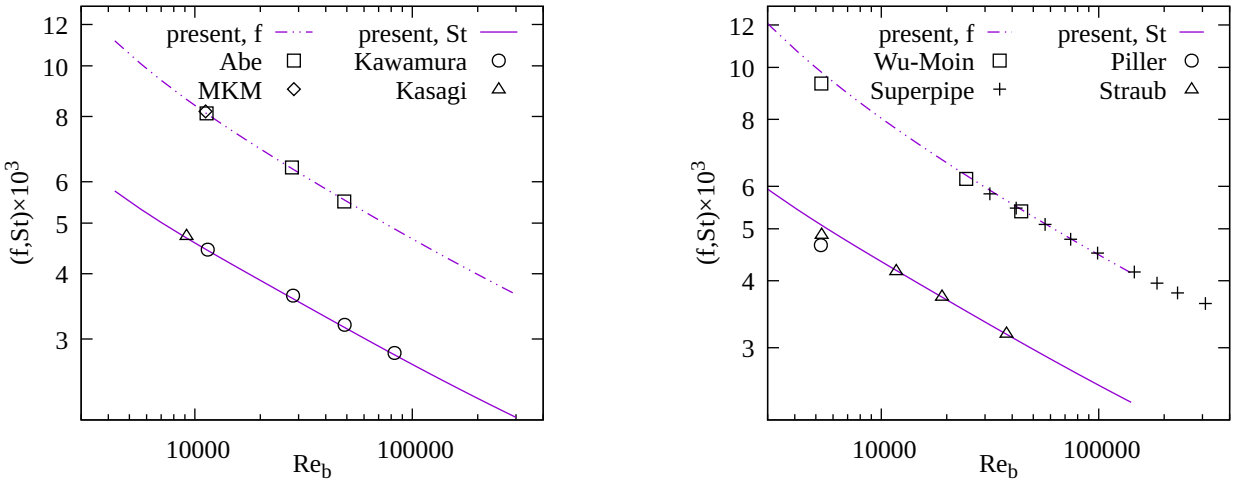

(a) Turbulent plane channel flow (DNS of [37][38][39][40][41]) (CP, (H) BC)

(b) Turbulent round pipe flow (DNS of [42][43][44], experiment of [45]) (CP, (H) BC)

Figure 2: Friction factor and Stanton number predictions for 1D flows compared to DNS

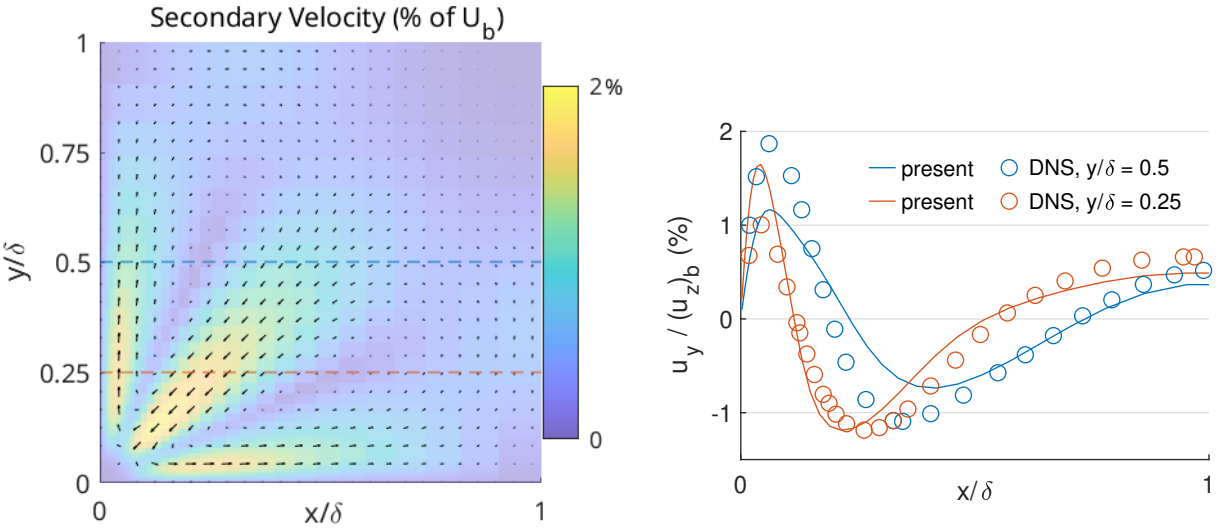

Figure 3: Secondary flow in the lower left quadrant of a square duct at $Re_b = 4,410$, compared to DNS [46] (contours: $|v_{sec}|/U_b$, %)

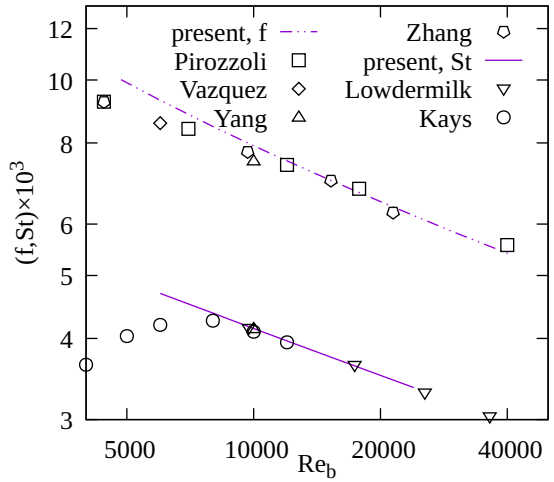

Figure 4: Friction factor and Stanton number predictions for turbulent square duct flow compared to DNS[46][47][48][49] and experiment[50][3] (CP, (H) BC)

3.4. Thermal Boundary Conditions

The boundary conditions applied to Equation (9) must constrain the solution to represent the flow through a specific cross-section of an evolving, but self similar, flow. This is enforced by setting the wall temperature and the distribution of local streamwise temperature gradient, $\frac{dT}{dz}$, as given by Equation (4).

To simulate a constant average heat flux boundary condition, (H), a uniform streamwise temperature gradient is set according to Equation (5):

$$\frac{dT}{dz} = \frac{dT_w}{dz} = \frac{dT_b}{dz} \tag{17}$$

As wall temperature evolves in unison with bulk temperature under (H) conditions, specifying the local wall temperature defines the streamwise position represented by the sectional flow.

To simulate a constant wall temperature boundary condition, (T), a uniform *normalised* streamwise temperature gradient is set according to Equation (5):

$$\frac{dT}{dz} = \frac{T_w - T}{T_w - T_b}\frac{dT_b}{dz} \tag{18}$$

As bulk temperature gradient decays exponentially in the streamwise direction, specifying the local $\frac{dT_b}{dz}$ defines the streamwise position represented by the sectional flow.

4. Results and Discussion

4.1. Thermal Boundary Conditions

In an idealised low-speed flow with constant properties, the dissipation term in Equation (9) is zero and the diffusivity is independent of temperature. Therefore, the temperature distribution (thus HTC) for a given flow is determined by the distribution of the convection term. Figure 5 shows the distribution of the convection term for a laminar channel flow under the (H) and (T) BCs. For the (T) BC, this term can be seen to attenuate toward the wall as $T \rightarrow T_w$, causing a shallower near-wall temperature gradient than for (H). This results in St_H exceeding St_T for laminar flows by 9.5% in plane channels, and 19.6% in pipes. These results are in agreement with analysis [2].

Figure 6 shows a similar comparison for a turbulent channel flow. Here, the majority of the thermal resistance occurs in a thin sub-layer by the wall. This reduces the sensitivity of the temperature field to the wider distribution of convection over the section, reducing the difference between St_H and St_T. This is reflected in the results shown in Figure 7, where $\frac{St_H}{St_T}$ reduces at higher Reynolds numbers and lower shape factors, as the viscous sub-layer becomes less and less significant.

The St_H/St_T predictions for turbulent pipe flow shown in Figure 7 show reasonable agreement with DNS[44], and with the ~1-4% observed in experiments[2][51]. This small BC effect on HTC becomes pertinent when analysing small sensitivities, which has led to the notion that improper comparison of (H) and (T) data has misled analyses of property gradient effects[8].

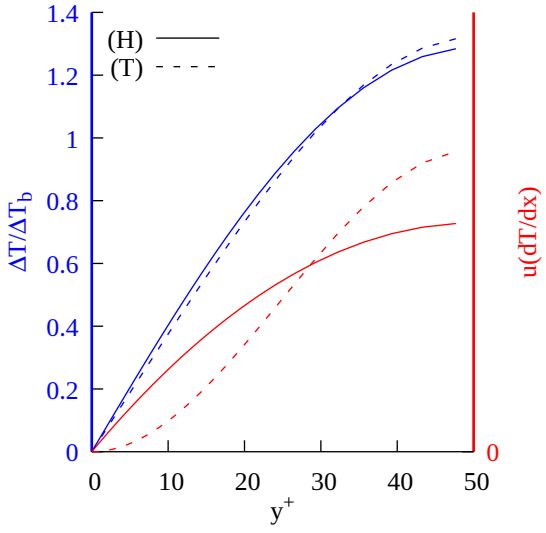

Figure 5: Temperature profiles and convection budget for a heated laminar 1D channel, $Re_\tau = 50$

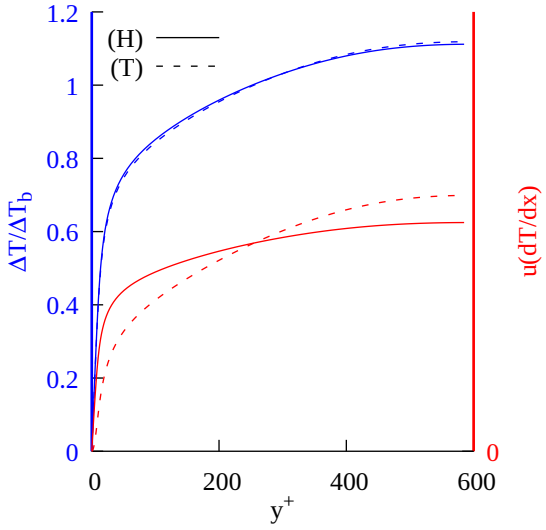

Figure 6: Temperature profiles and convection budget for a heated turbulent 1D channel, $Re_\tau = 590$

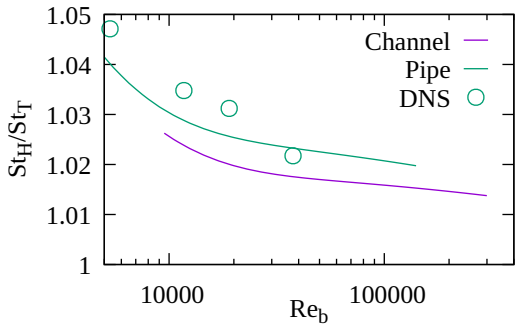

Figure 7: St_H/St_T for turbulent 1D pipe and channel flows, with pipe DNS[44]

4.2. Dissipation

In a constant property flow governed by Equation (9), the diffusivity remains independent of temperature, therefore the temperature field is determined by the distribution of the convection and dissipation terms. Figure 8 shows how the dissipation term is distributed in comparison to the convection term (under (H) thermal BC) for a turbulent channel flow. Also shown are the temperature distributions which arise due to each term:

- Temperature field ΔT_D is produced by the dissipation term in (9), with the convection term set to zero (I.E. $\frac{dT_b}{dz}$=0)
  - These conditions are denoted (D) henceforth
- Temperature field ΔT_H, is produced by the (H) BC with dissipation set to zero

The two terms are distributed very differently, with the convection term acting predominatly near the mid-channel while the dissipation term is strongest in the high-strain region near the wall. This results in a significantly steeper near-wall temperature gradient for case (D) compared to (H).

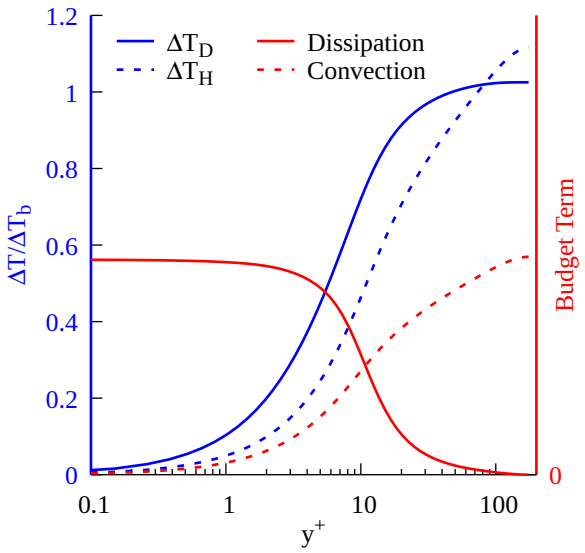

Figure 8: Normalised temperature profiles produced under (D) and (H) BCs, and the convection and dissipation terms in (9) for a 1D, constant property turbulent channel flow, Re_τ=180

The steeper temperature gradient at the wall results in the dissipation-heated flows having a higher HTC than the flow heated/cooled by streamwise temperature gradient. This can be seen in Figure 9, where the Stanton numbers computed for flows under condition (D) are shown to be approximately twice that of flows under (H) BCs for Pr~1. While St_D/St_H decreases with Prandtl number for turbulent flows, for laminar flows St_D/St_H is independent of Pr. The St_D/St_H values of 2.2 and 2.1 computed for laminar pipes and channels respectively are in agreement with analyses [18] and [15].

In more general flows, both convection and dissipation influence the temperature field. The integral contributions of these terms sum to the total heat flux at the wall, $\dot{q}$. The contribution

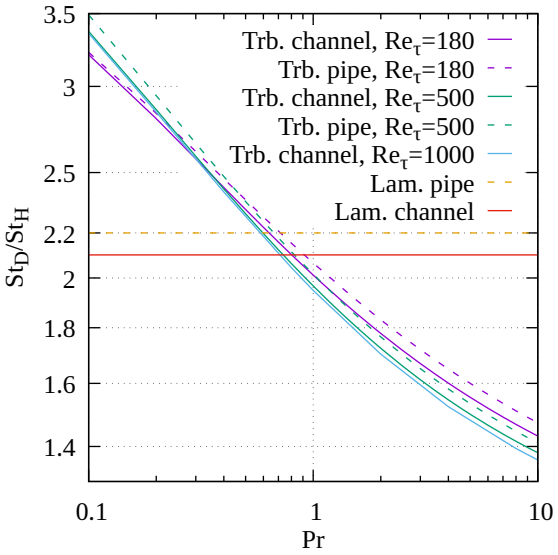

Figure 9: Ratio of Stanton numbers between dissipation and convection (H) driven heating for 1D, constant property flows at various Prandtl numbers

from the convection term is given by:

$$\dot{q}_H = (\rho u)_b c_p \frac{dT_b}{dz} \frac{Area}{Perimeter} \tag{19}$$

While the contribution from the dissipation term is given by:

$$\dot{q}_D = -u_b \frac{dp}{dz} \frac{\text{Area}}{\text{Perimeter}} = \frac{1}{2}\rho u_b^3 f \tag{20}$$

It is convenient to express the relative significance of these mechanisms by the ratio[4]:

$$Qr = -\frac{\dot{q}_H}{\dot{q}_D} \approx \frac{c_p \frac{dT}{dz}}{-\frac{1}{\rho_b}\frac{dp}{dz}} = \frac{\left(\begin{array}{c}\text{Enthalpy}\\ \text{Rise}\end{array}\right)}{\left(\begin{array}{c}\text{Pumping}\\ \text{Work}\end{array}\right)} \tag{21}$$

Figure 10&11 show how temperature distribution and Stanton number change as Qr is varied for a turbulent channel flow They may be described as follows:

1. $Qr \leq 0$: Both dissipation and convection supply heat to the section, causing St to smoothly transition from St_H to St_D as Qr goes from $-\infty$ to 0
2. $Qr = 0$: Dissipation in thermal equilibrium, $St = St_D$
3. $Qr > 0$: The fluid begins to absorb the heat of dissipation
4. Qr~0.5: The opposing source (dissipation) and sink (convection) terms lead to non-monotonic temperature profiles, causing a singularity in St as T_b crosses T_w
5. $Qr = 1$: Adiabatic condition: all dissipated heat absorbed
6. $Qr > 1$: Net cooling, St converges to St_H as Qr goes to ∞

[4] Qr can be related to Brinkman number as used in [15] $Qr = 1 - 2/Re_b f Br_q$

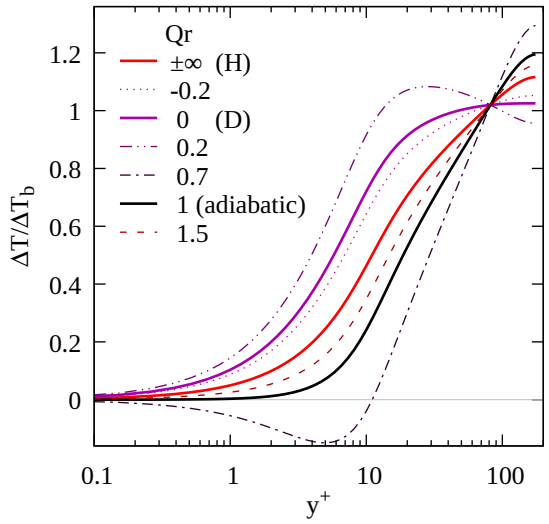

Figure 10: Normalised ΔT profiles for mixed dissipative-convective(H) heating/cooling of a CP 1D turbulent channel flow, Re_τ=180

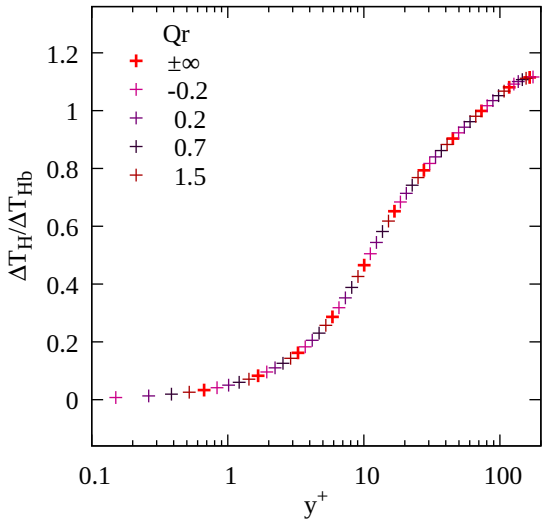

Figure 12: Normalised ΔT_H profiles for mixed dissipative-convective(H) heating/cooling of a 1D, constant property turbulent channel flow, Re_τ=180

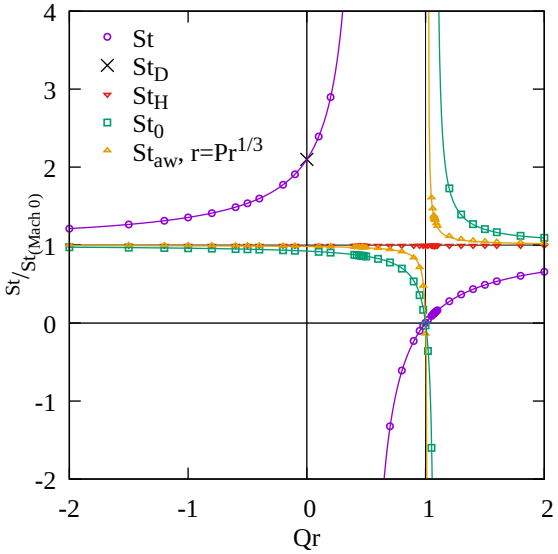

Figure 11: Static, stagnation, convective, and dissipative Stanton numbers over a range of Qr for a CP 1D turbulent channel flow at Re_τ=1000

4.2.1. Decomposition of the Temperature Field

Clearly, the temperature field cannot be effectively characterised by a single HTC (defined as (1)) for $Qr{\sim}1$. Fortunately, the linearity[5] of Equation (9) in T allows the temperature field to be decomposed as follows:

$$\Delta T = \Delta T_H + \Delta T_D \qquad \Delta T_b = \Delta T_{Hb} + \Delta T_{Db} \tag{22}$$

Where ΔT_H is the temperature field component due to the convection term in (9), and ΔT_D is the temperature field component due to the dissipation term. Figure 12 demonstrates the validity of this decomposition, where ΔT_D (the ΔT field at Qr=0) is subtracted from the ΔT fields shown in Figure 10 to isolate dissipation-invariant distributions, ΔT_H.

[5] When properties are held constant

ΔT_H and ΔT_D relate to partial heat fluxes (19,20) by HTCs:

$$\dot{q}_H = h_H \Delta T_{Hb} \qquad \dot{q}_D = h_D \Delta T_{Db} \tag{23}$$

Substitution of (23) into (22) allows St_H to be expressed as:

$$St_H = \frac{\dot{q} - \dot{q}_D}{G c_p \Delta T_b - \frac{\dot{q}_D}{St_D}} \tag{24}$$

This formula allows the ideal (passive temperature) Stanton number to be obtained from non-ideal (finite Qr) results using the Stanton number obtained with $Qr = 0$. Figure 11 shows the results produced by (24) to be invariant to Qr.

4.2.2. Recovery Factor

It is discussed in section 2.3 that heat transfer with dissipation may be well-characterised by a the low speed HTC (I.E. h_H) if temperatures are referenced to T_{aw}. This method is more convenient than Equation (24), in that auxilliary information about St_D is not required, as the adiabatic wall temperature may be calculated via (6) with an appropriate correlation for recovery factor. The St_{aw} results shown on Figure 11 are calculated in this manner. St_{aw} is well isolated from dissipation effects over most of the plot, however as Qr approaches 1, St_{aw} becomes erratic. This behaviour may be analysed via the decomposed temperature field.

The adiabatic wall condition may be expressed, via (23), as:

$$0 = \dot{q}_H + \dot{q}_D = h_H(\underbrace{T_b - T_{aw}}_{\Delta T_b} - \Delta T_{Db}) + h_D \Delta T_{Db}$$

$$\rightarrow T_{aw} = T_b + \underbrace{\Delta T_{Db}\left(\frac{h_D}{h_H} - 1\right)}_{\delta T_r} \tag{25}$$

where δT_r is temperature recovery. By relating $\dot{q}_D$ to f via (20),

δT_r may be cast in terms of a recovery factor as given by (6)[6] :

$$\delta T_r = \frac{\dot{q}_D}{h_D}\left(\frac{1}{h_H} - \frac{1}{h_D}\right) = \frac{1}{2c_p}\underbrace{\left(\frac{f}{St_H} - \frac{f}{St_D}\right)}_{r'_b} u_b^2 \tag{26}$$

$$= \underbrace{\left(\frac{f}{St_H} - \frac{f}{St_D}\right)\frac{u_b^2}{(u^2)_b}}_{r_b}(T_{0b} - T_b) \tag{27}$$

It can be shown that the heat flux predicted by (1) using the low speed HTC($\equiv h_H$) is exact when referenced to T_{aw}:

$$h_H(T_{aw} - T_w) = h_H\left(\Delta T_b + \Delta T_{Db}\left(\frac{h_D}{h_H} - 1\right)\right)$$
$$= h_H\Delta T_H + h_D\Delta T_{Db} \equiv \dot{q}_H + \dot{q}_D \tag{28}$$

However, it should be noted that r_b values obtained through correlations will be inexact. If the *estimated* r_b is defined as $\hat{r}_b = (1+\epsilon)r_b$, where ϵ is the error, the resulting T_{aw} estimate produces an HTC given by:

$$h_{\hat{aw}} = \frac{\dot{q}}{\underbrace{T_b + (1+\epsilon)\delta T_r}_{\hat{T_{aw}}} - T_w} = h_H\left(1 - \frac{\epsilon}{\epsilon + \frac{1-Qr}{1-\frac{h_H}{h_D}}}\right) \tag{29}$$

Equation (29) is shown as solid lines in Figure 11, and can be seen to fit the data well. The ϵ for each St definition is calculated relative to the true r_b according to (27) (0.862 for this flow):

- St: Equivalent to $\hat{r}_b = 0$, giving $\epsilon = -100\%$
- St_0: Equivalent to $\hat{r}_b = 1$, giving $\epsilon = {}^1/_{0.862} - 1 = 16\%$
- St_{aw}: $\hat{r}_b = \sqrt[3]{Pr} = 0.892$, giving $\epsilon = {}^{0.892}/_{0.862} - 1 = 3.5\%$

It is notable that Equation (27) forms r_b in terms of f and St, whereas in most prevalent correlations r is determined entirely by Pr[2][24]. However, it is well known[2] that f and St_H are highly correlated, with the scaling between the two usually being well characterised by some power upon Pr[53]. With St_D/St_H shown to also being well characterised by Pr, it can be seen how r'_b in (26) also reduces to a function primarily of Prandtl number. The nonuniformity factor, ${}^{u_b^2}/_{(u^2)_b}$, in (27) is discussed by [54][55], and is specific to recovery factors referenced to bulk quantities. The recovery factors computed for several flows are shown in Figure 13. The importance of using internal flow correlations is most clear for the laminar results, which are clearly better characterised by $r_b \sim Pr$ given by [26] for pipes than by the $r_b \sim \sqrt{Pr}$ correlation [2][24] for external boundary layers. The recovery factors for turbulent flows can be seen to scale to lower powers of Pr as Re increases; it might be expected that, as Re increases and $r'_b \to r_b$[54], the turbulent recovery factors would approach the external flow correlation $r_b \sim Pr^{1/3}$ by [56]. However, the results show r_b to scale with Pr to a power less than ${}^1/_3$ at the highest Reynolds numbers. Given that the recovery factors all align with the experimental range given by [19], it is possible that this is simply an artefact of the Pr_T model (13) being calibrated for air[2]. However, as seen in laminar studies [26], this may also suggest that some of the assumptions underpinning the external flow correlation may break down for internal flows.

[6] r'_b differs from r_b in that Equation (26) is referenced to u_b^2 (due to the definition of f[3]), whereas T_0 is referenced to $(u^2)_b$ [52]. This distinction is increasingly important at lower Re as the velocity profile becomes sharper.

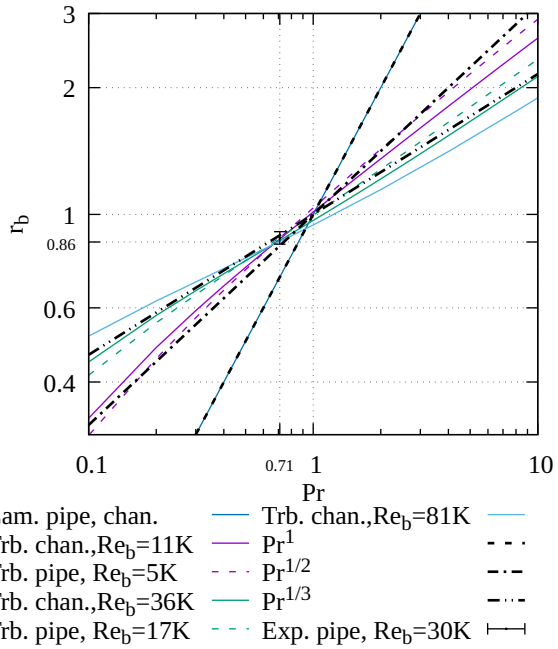

Figure 13: Recovery factors evaluated by Equation (27) from 1D pipe and channel computations, with experimental result by [19]

4.3. Variable Property Effects

The separate and combined effects of introducing variable density and viscosity to the model for a turbulent channel flow are shown in Figure 14. As seen in [30], the dominant effect of heating is an increase in eddy viscosity away from the wall due to density gradient. This decrease in mid-channel velocity results in a reduction in Re_b for a given Re_τ.

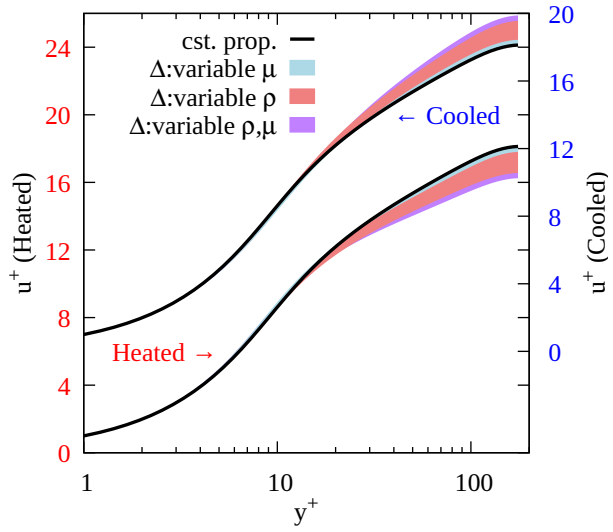

Figure 14: Change in velocity profile in a turbulent 1D channel due to variable viscosity and density effects (air, $Re_\tau = 180$)

The y^+-t^+ profile for a given Re_τ changes similarly, however it should be noted that HTCs are determined by the (y/δ)-$(\Delta T/\Delta T_b)$ profile, and correlations are referenced to Re_b. Reference to bulk quantities adds additional ρ dependence; heating a flow causes density to increase away from the wall, weighting bulk quantities toward mid-channel values. The summary effect of this can be seen in the outer-scaled bulk-normalised temperature profiles at controlled Re_b, shown in Figure 15. This shows heating to result in reduced near-wall temperature gradient, thus a reduced HTC (as seen by [30]). Examples of how HTC varies with heating/cooling are shown in Figure 16.

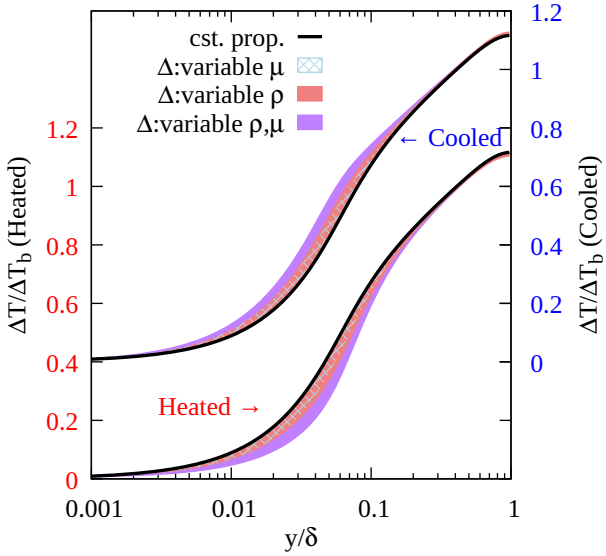

Figure 15: Change in temperature profile in a turbulent 1D channel due to variable viscosity and density effects (air, $Re_b = 11,310$)

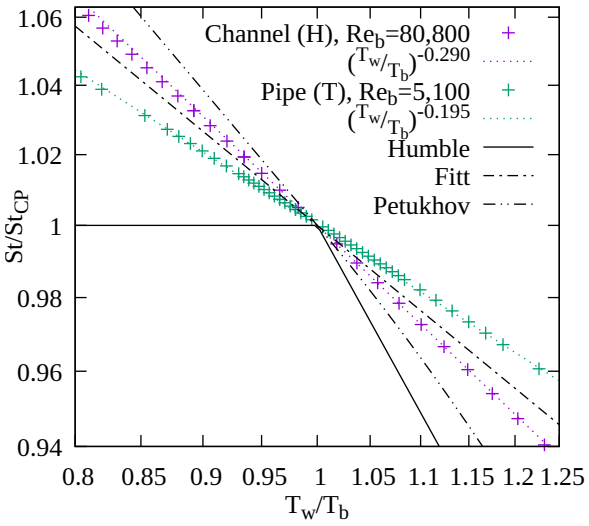

Figure 16: Variation of Stanton number with wall temperature for variable property 1D flows at fixed Re_b, alongside [4][31][7] (see Table 1)

4.3.1. Power-Law Correction Factor

T_w/T_b-St results for $0.8<\frac{T_w}{T_b}<1.2$ have been computed for a range of geometries and Reynolds numbers. These results were found to be well characterised by power-law fits of the form (7), as illustrated by the 2 examples shown in figure 16. The exponent, n is found to be relatively invariant to T_w/T_b, exhibiting neither the smooth variation with T_w/T_b predicted by Petukhov[7], nor the heating-cooling discontinuity posited by Humble[4]. As such, the present results support the notion (discussed in section 2.4) that discontinuous forms of (7) are artefacts arising from inconsistencies between heated and cooled flow experiments.

Having shown that property gradients affect the viscous and turbulent regions of the flow differently, one may expect the relative significance of these regions to affect the flow's overall sensitivity to temperature gradient. This manifests as a variation of n between boundary conditions, geometries, and Reynolds numbers. Figure 17 shows the best-fit value of n obtained over the range of cases computed, showing boundary condition, geometry, and Reynolds number to each have a significant effect. Thus, the present results challenge the assumption by [3][7][4] that a precise universal n can be defined. That being said, the present results are in closest agreement to the results obtained by [31]; interestingly, this is the only surveyed reference which employs a consistent methodology between $T_w > T_b$ and $T_w < T_b$ tests.

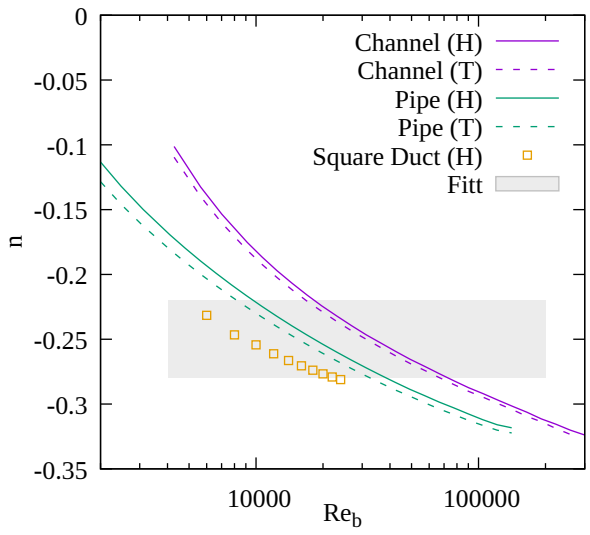

Figure 17: Variation of best fit exponent for Equation (7) with Reynolds number alongside results of [31]

4.3.2. Modified Reference Quantities

An often-cited advantage of the above method for property correction is that it allows the following unambiguous definition of bulk Reynolds number[3] to be retained:

$$Re_b = \frac{(\rho u)_b D_h}{\mu_{T_b}}, \qquad (\rho u)_b = \frac{\dot{m}}{A} \qquad (30)$$

Whereas when modified reference quantities are employed, $(\rho u)_b$ must be decomposed into ρ_b and u_b:

$$(\rho u)_b = \frac{1}{A}\int_A \rho u dA = \rho_b \times \underbrace{\frac{\frac{1}{A}\int_A \rho u dA}{\rho_b}}_{u_b} \tag{31}$$

where ρ_b is defined by (15) with p set to $\overline{p} = \int p dA$ and T set to T_b [4]. Retaining $\overline{p}$, alternate values of ρ and μ may be specified by evaluating (15) and (16) at a film temperature, defined as:

$$T_\lambda = (1-\lambda)T_w + \lambda T_b, \qquad \lambda \in [0,1] \tag{32}$$

μ and ρ appear a total of 4 times in the definitions of Re, f, and St, thus a reference framework may be described by 4 λ values, i, j, k, and l. These are defined as presented in equations (33-36). Such quantities are of use in cases where the flow is better characterised by properties at a temperature other than T_b. Several popular referencing configurations are given in Table 3.

Formulations B-E are the conventionally defined[30] *modified film* quantities where all properties are evaluated at a single film temperature. G is a conventionally defined *film* quantity where $(\rho u)_b$ may be retained and only μ modified. F has been added by the author on the basis:

- Viscous stress/diffusion peaks *at* the wall: $\mu_{ref} = \mu_{\text{wall}}$
- Turbulent stress/diffusion peaks *near* the wall: $\rho_{ref} = \rho_{0.4}$

$$Re_{i,j} = \frac{\rho_i u_b D_h}{\mu_j} = \left(\frac{\rho_i}{\rho_b}\right)\left(\frac{\mu_b}{\mu_j}\right) \times Re_b \tag{33}$$

$$f_k = \frac{\overline{\tau_w}}{\frac{1}{2}\rho_k u_b^2} = \left(\frac{\rho_b}{\rho_k}\right) \times f_b \tag{34}$$

$$Nu_l = \frac{hD_h}{k_l} = \frac{hD_h Pr}{\mu_l c_p} = \left(\frac{\mu_b}{\mu_l}\right) \times Nu_b \tag{35}$$

$$St_{i,j,l} = \frac{Nu_l}{Re_{mi,j}Pr} = \frac{h\frac{\mu_j}{\mu_l}}{\rho_i u_b c_p} = \left(\frac{\rho_b}{\rho_i}\right)\left(\frac{\mu_j}{\mu_l}\right) \times St_b \tag{36}$$

	i	j	k	l	ref.
A	1.0	1.0	1.0	1.0	(bulk)
B	0.0	0.0	0.0	0.0	[4]
C	0.4	0.4	0.4	0.4	[30]
D	0.5	0.5	0.5	0.5	[30]
E	0.6	0.6	0.6	0.6	[30]
F	0.4	0.0	0.4	0.4	Present
G	1.0	0.5	-	1.0	[33]

Table 3: λ values for reference quantity definitions under investigation

The usefuless of a reference formulation is determined by its ability to map variable property results onto a constant property characteristic. The investigations cited in Table 3 assess this ability based upon databases of HTCs at a limited number of temperature ratios, which suffer from the experimental inconsistencies discussed in section 2.4. To assess these modified characteristics over a more complete range of conditions, *Re-f-St* computations are performed for $0.8 < \frac{T_w}{T_b} < 1.2$ at fixed Re_b. This is repeated for several values of Re_b, the results of which are plotted for definitions A-G (see Table 3) in Figure 18.

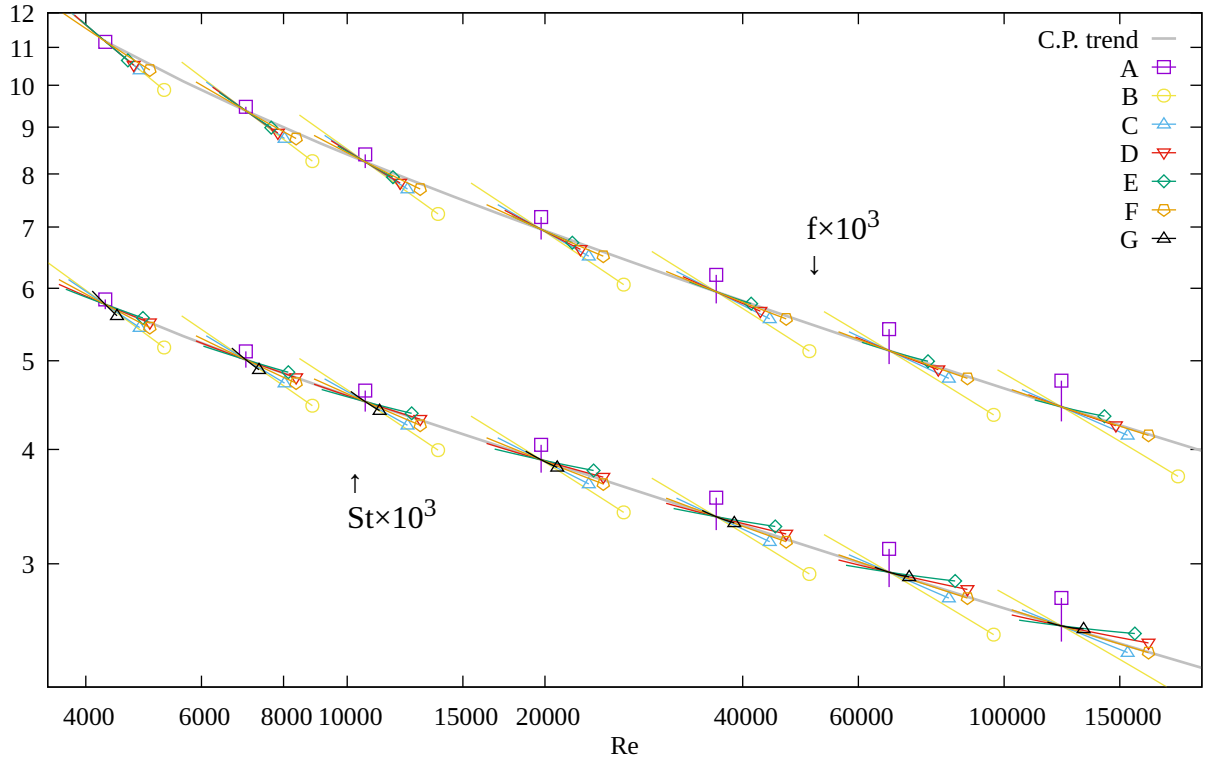

Figure 18: *Re-f* & *Re-St* characteristics produced by varying heat flow to a 1D channel (H) at several fixed Re_b, Symbols at $T_w/T_b \sim 0.8$

Figure 18 shows the *film* referencing of G[33] to achieve minimal displacement from the CP solution, however the characteristics do not align well with CP trend line. The *modified film* referencing of [30](C-E) is more effective at aligning the characteristics with the CP trend-line. Of these forms, no single λ achieves consistent alignment with the constant property trendlines throughout the domain of Re, however $\lambda = 0.5$ (D) gives the best compromise for both f and St (This is also the conclusion reached by [30]). The new formulation, F, gives much more consistent alignment for both f and St. This implies that the surface viscosity provides a better characterisation of the thermal and mechanical flow that the film viscosities used by [30][33].

Formulations D, F, and G demonstrate the ability to mitigate T_w/T_b sensitivity for Re-f-St correlations, in that changing T_w/T_b moves *along* the CP characteristic rather than departing from it. As the most effective formulation, F is adopted henceforth, subscripted $_{mf}$. Similar results for pipe flows (see A.23, A.24) indicate that this effectiveness is retained for different geometries and thermal boundary conditions.

4.4. Application to Complex 2D Flows

To assess the proposed methods, square duct simulations are performed at a range of Reynolds numbers and streamwise temperature gradients. The unprocessed results are shown in Figure 19, where the spread of the data illustrates the inadequacy of "naive" Re-St correlations for variable property flows.

It is clear that the results shown in Figure 19 do not converge toward the constant property characteristic as temperature gradient is reduced. This "deflection" of results away from the constant property characteristic at low Qr is best explained by looking at a single Re_b, shown in Figure 20. This shows how dissipation (as Figure 11) and property gradient (as Figure 16) effects to combine in a way which prevents $St \rightarrow St_H$.

Figure 20 suggests that, if not accounted for, dissipation distorts the T_w/T_b-St characteristic by reducing gradient and adding a discontinuity. This may explain the reduced property variation and heating-cooling discrepancy observed by [8] between heated[4][7] and cooled[5][6] flow experiments.

4.5. Applying Corrections to 2D Re-St Correlations

The scatter between computed characteristics shown in Figure 19 summarises the problem sections 4.1-4.3 aim to address. The effectiveness of these methods may therefore be evaluated by their ability to reduce this scatter, presented in Figure 21.

4.5.1. Dissipation Rejection

With geometry and fluid properties fixed, frictional heating scales with Reynolds number, resulting in the magnitude of Qr decreasing with Re_b for a fixed dT_b/dz. This makes it non-trivial for test campaigns at fixed temperature gradients to avoid problematic Qr values over large Re_b ranges. The minimum and maximum Qr values for the present datasets are given in Table 4. Figure 19 shows low Qr datasets to converge toward the St_D characteristic ('0') at high Re_b - this is a symptom of this inverse relation between Re_b and Qr.

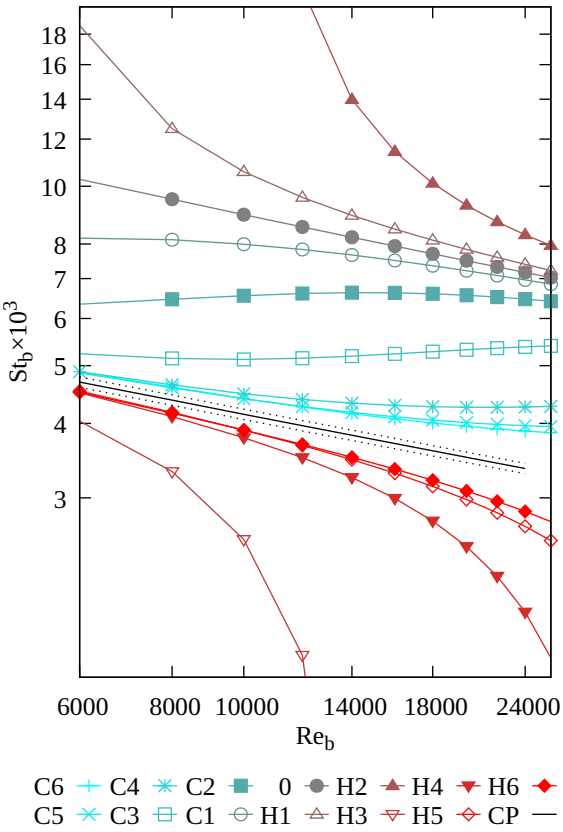

Figure 19: Re_b-St_b computations at a range of dT/dz (see Table 4) for a variable property turbulent square duct under (H) BCs, Mach 0.1-0.3

	T_w/T_b	Qr		T_w/T_b	Qr
$C6$	0.81, 0.87	-50, -5	$C5$	0.85, 0.91	-35, -3
$C4$	0.92, 0.95	-17, -1.5	$C3$	0.966, 0.988	-4, -0.2
$C2$	0.977, 0.996	-1.1, -.1	$C1$	0.980, 0.998	-0.26, -.01
0	0.981, 0.999	0			
$H1$	0.984, 1.000	0.03, .27	$H2$	0.987, 1.001	0.1, 1.1
$H3$	1.001, 1.009	0.2, 4	$H4$	1.04, 1.05	1.5, 17
$H5$	1.09, 1.11	3, 35	$H6$	1.13, 1.18	5, 55

Table 4: Temperature and dissipation ratio ranges for the fixed dT/dz datasets

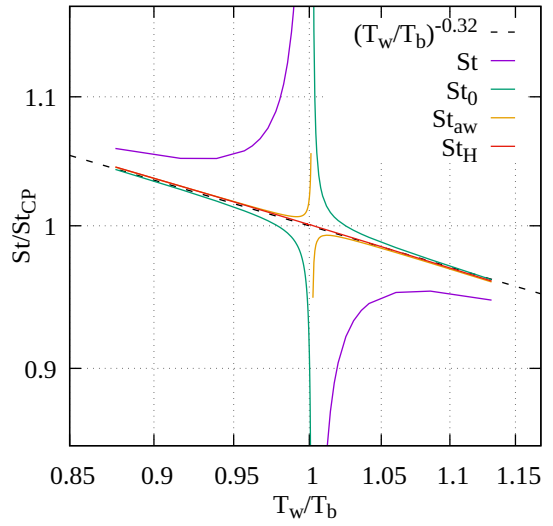

Figure 20: Variation of Stanton number with wall temperature for variable property turbulent square duct flow at fixed $Re_b = 7,000$, Mach 0.1

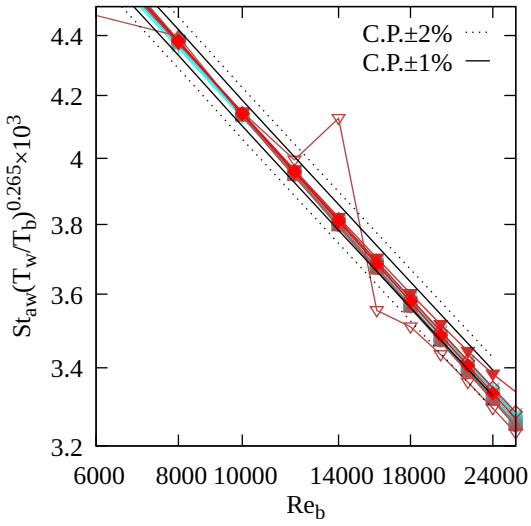

(a) HTC referenced to T_{aw} with $r_b = \sqrt[3]{Pr}$, corrected by power law (7) with $n = -0.265$

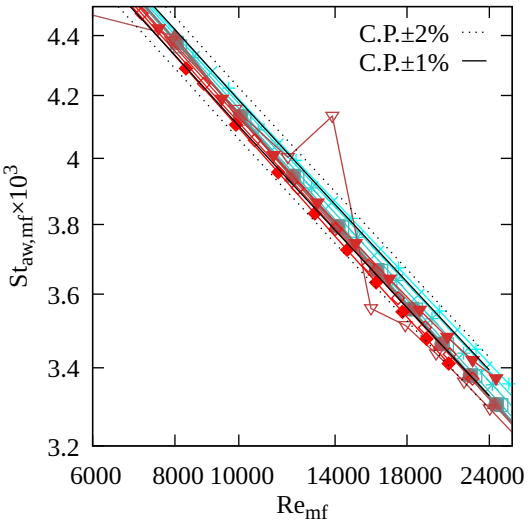

(b) HTC referenced to T_{aw} with $r_b = \sqrt[3]{Pr}$, mapped to film reference F (see Table 3)

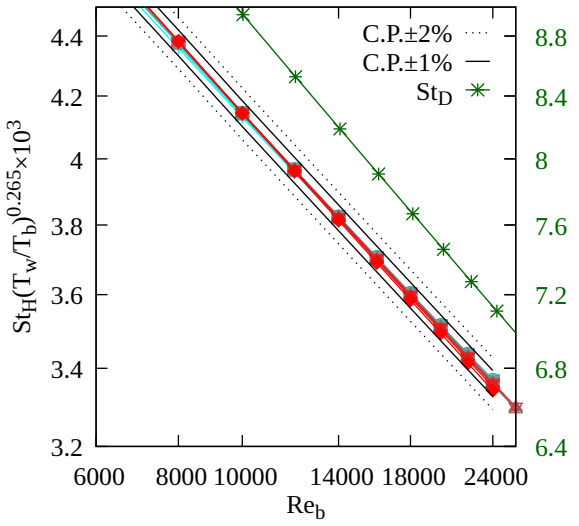

(c) Convective HTC (24), corrected by power law (7) with $n = -0.265$

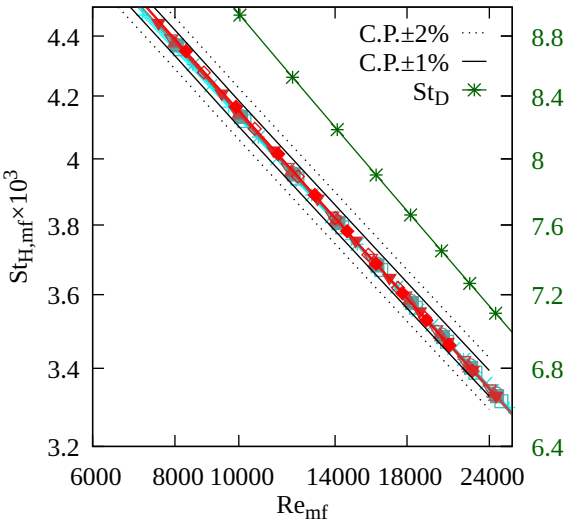

(d) Convective HTC (24) mapped to film reference F (see Table 3)

Figure 21: Corrected *Re-St* characteristics for a variable property turbulent square duct under (H) BCs, Mach 0.1-0.3 (see Figure 19 for legend)

Figures 21a&21b show the Stanton numbers corrected using $r_b = \sqrt[3]{Pr}$. Where $|Qr-1| \gg 1$, this can be seen to cluster results toward a single characteristic quite effectively, however the correction breaks down close to the adiabatic condition. In general, this causes the scatter between characteristics to increase at higher Re_b as Qr moves toward zero. An extreme deviation from the CP characteristic is apparent in dataset H3 near Re_b=14,000, as H3 passes through $Qr \sim 1$.

Figure 21c shows the results obtained using Equation (24), where St_D is obtained by interpolating data set 0 using $_{mf}$ property referencing. This method is more effective than the former, unconditionally collapsing results onto a single characteristic with less than 0.5% scatter.

4.5.2. Property Variation

Figure 21c&21d show that, when paired with effective dissipation rejection, both the power-correction and film-quantity methods condense results to a single line with less that 0.5% scatter. Figure 17 shows that the property exponent for the square duct is lower than for a pipe or channel, but exhibits the same downward trend with *Re*. The characteristic shown in Figure 21c is corrected using the average n of -0.265, which was found to no less effective than using $n{=}fn(Re)$ in the range investigated. This may explain the perceived adequacy of constant-power corrections[3] for small temperature differences and *Re* ranges.

It may be noted that the results shown in Figure 21a&21b increase in scatter and deviate slightly below the constant property characteristic at high Reynolds numbers. This is likely due to variable property corrections being calibrated to (H)/(T)-driven temperature fields: With dissipation becoming significant in the higher *Re* results, the temperature profiles deviate from those produced under ideal (H)/(T) conditions, thus the variable property corrections are less accurate. This effect is less pronounced in Figures 21c&21d, indicating that the film-referenced St_D characteristic captures the effect of property

variation on dissipative heating more robustly than a fixed r_b value. This issue is addressed in empirical work [20] by adding a kinetic term to the film temperature definition.

4.5.3. Data Requirements

While characterisation by the power-law and film-quantity methods are on par in terms of efficacy, it is important to note that the power law method is less convenient: data for a range of T_w/T_b must be obtained at controlled Re_b in order to fit exponent n. The film-quantity method is more general, allowing scattered data for a single heat flow to fully define a *Re-St* correlation. Similarly, the disadvantage of the dual-coefficient method for dissipation accounting is that rather than using universal correlations for recovery factor, auxiliary *geometry-specific* data is required. It should be noted that while this auxiliary data takes the form of a $Re\text{-}St_D$ in this work, Equation (27) shows that similar performance may be achieved via a geometry-specific $Re\text{-}r_b$ correlation.

4.5.4. Friction Factor

For completeness, Figure 22 shows the film correction applied to friction factor. This shows film reference F to also be effective at condensing *Re-f* data to a single characteristic, with a scatter of ±0.5% for $0.8 < {}^{T_w}/_{T_b} < 1.2$.

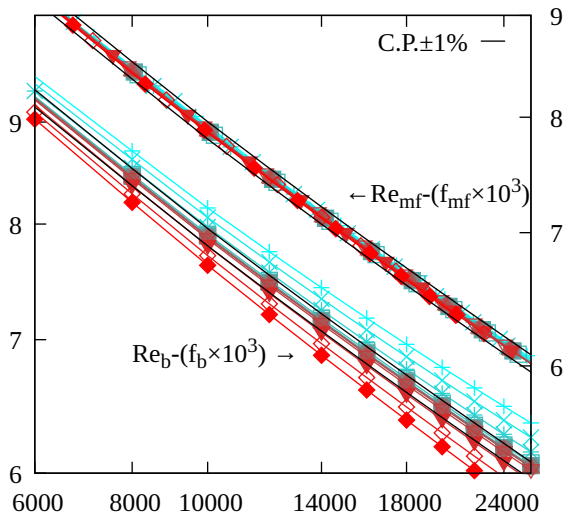

Figure 22: Square duct friction factor results (see Figure 19 legend)

5. Conclusions

The methods presented in this work improve the robustness of *Re-St* correlations for predicting heat transfer to/from fully developed flows where dissipation or property variation are significant. Accounting for such features mitigates them as a source of uncertainty, allowing heat exchanger matrix geometries to be rapidly characterised by CFD. These advantages improve the flexibility and reliability of correlation-based modelling in design.

The present investigation focuses upon air-like gasses at moderate temperatures, where the 3 mechanisms discussed are of secondary significance. However, their significance may be expected to increase at lower Prandtl numbers (e.g.liquid metals)[2], lower absolute temperatures (e.g.cryogenic flows), or higher heat fluxes.

5.1. Thermal Boundary Conditions

A simple methodology for representing constant heat flux and constant wall temperature conditions for fully developed flows is presented. While the constant heat flux formulation is widespread in CFD[57][58], the constant wall temperature formulation differs from most CFD studies of such[59][60][61] in that it doesn't require redefinition of the transport equations, easing implementation. The formulations successfully reproduce the difference between (H) and (T) HTCs seen in both laminar[2] and turbulent[44] studies. These results highlight the importance of controlling boundary conditions when comparing/validating against any experimental data.

5.2. Dissipation

The results presented demonstrate HTC to be sensitive to dissipative heating as temperature ratios approach unity, even when Mach number is low. The conventional method, where adiabatic wall temperature is estimated via universal correlations, is shown to be effective so long as dissipation makes up less than 10% of the total heat flow. An alternative method, where separate HTCs are evaluated for convection and dissipation, was found to isolate dissipation more robustly. This method requires auxiliary results to determine the dissipative Stanton number, which was found to be ~ 2× the convective Stanton number for Pr~1.

5.3. Variable Property Effects

The present results are used to scrutinise several long-suspected[8] flaws in experimental investigations into property-gradient effects. This led to two key findings about power-law corrections:

- Power-law corrections are found to apply consistently between heated and cooled flows
- Exponents were seen to vary ($n \sim -0.25 \pm 0.05$) between geometries and operating points

The latter introduces the need for auxiliary *Re-n* correlations. For this reason, it is more convenient to instead account for property variation using modified reference quantities.

Modified film quantities were found to effectively capture for property gradient effects on both *Re-f* and *Re-St* correlations over the full range of geometries and boundary conditions investigated. The conventional modified film definition of [30] performed adequately in this regard, however better consistency was achieved with an improved formula (F, Table 3).

Acknowledgements

The authors gratefully acknowledge Rolls-Royce plc. for funding this work and granting permission for its publication. TD acknowledges funding from UKRI and Rolls-Royce plc. through the EPSRC Future Propulsion and Power CDT, EPSRC project reference 2640742.

References

[1] M. Ryemill, C. Bewick, R.-R. Plc, J. K. Min, The Rolls-Royce Plc Ultrafan Heat Management Challenge (2016).

[2] W. M. Kays, Convective Heat and Mass Transfer., 4th Edition, McGraw-Hill Series in Mechanical Engineering, McGraw-Hill Higher Education, Boston, 2005.

[3] W. M. Kays, A. London, Compact Heat Exchangers (3rd Edition), Scientific International, S.l., 1964.

[4] L. V. Humble, W. H. Lowdermilk, L. G. Desmon, Measurements of average heat-transfer and friction coefficients for subsonic flow of air in smooth tubes at high surface and fluid temperatures (Jan. 1951).

[5] W. B. Nicoll, W. M. Kays, The Influence of Temperature Dependent Properties on Gas Flow Heat Transfer in Circular Tubes - Technical Report No. 43, Tech. Rep. AD-227572, Stanford Univ., Calif. (Sep. 1959).

[6] T. Mizushina, T. Matsumoto, Shigeyuki. Yoneda, The effect of large temperature difference on the turbulent heat and momentum transfer in an air flow inside a circular tube, Journal of Chemical Engineering of Japan 9 (6) (1976) 450–457.

[7] B. Petukhov, Heat Transfer and Friction in Turbulent Pipe Flow with Variable Physical Properties, in: Advances in Heat Transfer, Vol. 6, Elsevier, 1970, pp. 503–564. doi:10.1016/S0065-2717(08)70153-9.

[8] D. M. McEligot, Convective Heat Transfer in Internal Gas Flows with Temperature-Dependent Properties., Tech. rep. (1982).

[9] F. P. Incropera, D. P. DeWitt, T. L. Bergman, A. S. Lavine (Eds.), Fundamentals of Heat and Mass Transfer, 6th Edition, Wiley, Hoboken, NJ, 2007.

[10] E. M. Sparrow, S. V. Patankar, Relationships Among Boundary Conditions and Nusselt Numbers for Thermally Developed Duct Flows, Journal of Heat Transfer 99 (3) (1977) 483–485. doi:10.1115/1.3450722.

[11] W. C. Reynolds, W. M. Kays, S. J. Kline, Heat Transfer in the Turbulent Incompressible Boundary Layer III - Arbitary Wall Temperature and Heat Flux, Tech. Rep. NASA-MEMO-12-3-58W (Dec. 1958).

[12] W. C. Reynolds, W. M. Kays, S. J. Kline, Heat Transfer in the Turbulent Incompressible Boundary Layer II - Step Wall Temperature Distribution, Tech. Rep. Rept-4995/PT2 (Dec. 1958).

[13] W. C. Reynolds, W. M. Kays, S. J. Kline, Heat Transfer in the Turbulent Incompressible Boundary Layer I - Constant Wall Temperature, Tech. Rep. NASA-MEMO-12-1-58W/PT1 (Dec. 1958).

[14] H. C. Brinkman, Heat effects in capillary flow I, Applied Scientific Research 2 (1) (1951) 120–124. doi:10.1007/BF00411976.

[15] O. Aydın, M. Avcı, Viscous-dissipation effects on the heat transfer in a Poiseuille flow, Applied Energy 83 (5) (2006) 495–512. doi:10.1016/j.apenergy.2005.03.003.

[16] P. M. Coelho, F. T. Pinho, A generalized Brinkman number for non-Newtonian duct flows, Journal of Non-Newtonian Fluid Mechanics 156 (3) (2009) 202–206. doi:10.1016/j.jnnfm.2008.07.001.

[17] J. Sheela-Francisca, C. P. Tso, Viscous dissipation effects on parallel plates with constant heat flux boundary conditions, International Communications in Heat and Mass Transfer 36 (3) (2009) 249–254. doi:10.1016/j.icheatmasstransfer.2008.11.003.

[18] G. L. Morini, M. Spiga, Nusselt Numbers in Rectangular Ducts With Laminar Viscous Dissipation, Journal of Heat Transfer 121 (4) (1999) 1083–1087. doi:10.1115/1.2826061.

[19] W. H. McAdams, Measurements of Recovery Factors and Coefficients of Heat Transfer in a Tube for Subsonic Flow of Air (985) (1945).

[20] E. R. G. Eckert, Engineering Relations for Heat Transfer and Friction in High-Velocity Laminar and Turbulent Boundary-Layer Flow Over Surfaces With Constant Pressure and Temperature, Journal of Fluids Engineering 78 (6) (1956) 1273–1283. doi:10.1115/1.4014011.

[21] A. C. Chambers, D. R. H. Gillespie, P. T. Ireland, G. M. Dailey, A Novel Transient Liquid Crystal Technique to Determine Heat Transfer Coefficient Distributions and Adiabatic Wall Temperature in a Three-Temperature Problem, Journal of Turbomachinery 125 (3) (2003) 538–546. doi:10.1115/1.1575252.

[22] R. Maffulli, L. He, Wall Temperature Effects on Heat Transfer Coefficient for High-Pressure Turbines, Journal of Propulsion and Power 30 (4) (2014) 1080–1090. doi:10.2514/1.B35126.

[23] J. Kaye, J. H. Keenan, W. H. McAdams, Report of Progress on Measurements of Friction Coefficients, Recovery Factors, and Heat-Transfer Coefficients for Supersonic Flow of Air in a Pipe, Transactions of the American Society of Mechanical Engineers 73 (3) (1951) 267–277. doi:10.1115/1.4016224.

[24] J. R. Stalder, M. W. Rubesin, T. Tendeland, A Determidation of the Laminar-, Transitional-, and Turbulent-Boundary-Layer Temperature-Recovery Factors on a Flat Plate in Supersonic Flow (1950).

[25] A. I. Leontiev, V. G. Lushchik, A. E. Yakubenko, The recovery factor in a supersonic flow of gas with a low Prandtl number, High Temperature 44 (2) (2006) 234–242. doi:10.1007/s10740-006-0029-8.

[26] J. C. Adams, J. C. Williams, Viscous compressible laminar flow in slender axisymmetric channels with adiabatic walls, Applied Scientific Research 21 (1) (1969) 113–137. doi:10.1007/bf00411601.

[27] L. He, Spectral Heat Transfer Coefficient for Thermal Design Analysis—Part 1: Augmenting the Cooling Law for Non-Isothermal Wall, Journal of Turbomachinery 147 (6) (Jun. 2025). doi:10.1115/1.4066671.

[28] W. Sutherland, LII. The viscosity of gases and molecular force, The London, Edinburgh and Dublin philosophical magazine and journal of science 36 (223) (1893) 507–531. doi:10.1080/14786449308620508.

[29] R. G. Deissler, Analytical Investigation of Fully Developed Laminar Flow in Tubes with Heat Transfer with Fluid Properties Variable Along the Radius (1951).

[30] R. G. Deissler, Analytical Investigation of Turbulent Flow in Smooth Tubes with Heat Transfer with Variable Fluid Properties for Prandtl Number Of 1 (1950).

[31] A. Fitt, C. Forth, B. Robertson, T. Jones, Temperature ratio effects in compressible turbulent boundary layers, International Journal of Heat and Mass Transfer 29 (1) (1986) 159–164. doi:10.1016/0017-9310(86)90045-1.

[32] J. P. Prideaux, The Experimental Determination of the Local and Average Heat Transfer Characteristics and Average Friction Coefficients for Turbulent Flow of Air and Argon with Variable Properties in Smooth Tubes with the Boundary Conditions of Constant Wall Temperature Heating and Increasing Heat Flux Heating, https://www.proquest.com/docview/302169034?pq-origsite=gscholar&fromopenview=true&sourcetype=Dissertations%20&%20Theses (1966).

[33] C. A. Sleicher, M. W. Rouse, A convenient correlation for heat transfer to constant and variable property fluids in turbulent pipe flow, International Journal of Heat and Mass Transfer 18 (5) (1975) 677–683. doi:10.1016/0017-9310(75)90279-3.

[34] K. Abe, Y.-J. Jang, M. Leschziner, An investigation of wall-anisotropy expressions and length-scale equations for non-linear eddy-viscosity models, International Journal of Heat and Fluid Flow 24 (2) (2003) 181–198. doi:10.1016/S0142-727X(02)00237-0.

[35] W. M. Kays, Turbulent Prandtl Number—Where Are We?, Journal of Heat Transfer 116 (2) (1994) 284–295. doi:10.1115/1.2911398.

[36] J. M. Weiss, W. A. Smith, Preconditioning applied to variable and constant density flows, AIAA Journal 33 (11) (1995) 2050–2057. doi:10.2514/3.12946.

[37] H. Abe, H. Kawamura, Y. Matsuo, Direct Numerical Simulation of a Fully Developed Turbulent Channel Flow With Respect to the Reynolds Number Dependence, Journal of Fluids Engineering 123 (2) (2001) 382–393. doi:10.1115/1.1366680.

[38] J. Kim, P. Moin, R. Moser, Turbulence statistics in fully developed channel flow at low Reynolds number, Journal of Fluid Mechanics 177 (1987) 133–166. doi:10.1017/S0022112087000892.

[39] R. D. Moser, J. Kim, N. N. Mansour, Direct numerical simulation of turbulent channel flow up to Ret=590 (1999).

[40] H. Kawamura, H. Abe, K. Shingai, DNS of turbulence and heat transport in a channel flow with different Reynolds and Prandtl numbers and boundary conditions (2000).

[41] N. Kasagi, Y. Tomita, A. Kuroda, Direct Numerical Simulation of Passive Scalar Field in a Turbulent Channel Flow, Journal of Heat Transfer 114 (3) (1992) 598–606. doi:10.1115/1.2911323.

[42] X. Wu, P. Moin, A direct numerical simulation study on the mean velocity characteristics in turbulent pipe flow, Journal of Fluid Mechanics 608 (2008) 81–112. doi:10.1017/S0022112008002085.

[43] M. Piller, Direct numerical simulation of turbulent forced convection in a pipe, International Journal for Numerical Methods in Fluids 49 (6) (2005) 583–602. doi:10.1002/fld.994.

[44] S. Straub, P. Forooghi, L. Marocco, T. Wetzel, R. Vinuesa, P. Schlatter, B. Frohnapfel, The influence of thermal boundary conditions on turbulent forced convection pipe flow at two Prandtl numbers, Interna-

tional Journal of Heat and Mass Transfer 144 (2019) 118601. doi:10.1016/j.ijheatmasstransfer.2019.118601.

[45] M. V. Zagarola, A. J. Smits, Scaling of the Mean Velocity Profile for Turbulent Pipe Flow, Physical Review Letters 78 (2) (1997) 239–242. doi:10.1103/PhysRevLett.78.239.

[46] S. Pirozzoli, D. Modesti, P. Orlandi, F. Grasso, Turbulence and secondary motions in square duct flow, Journal of Fluid Mechanics 840 (2018) 631–655. doi:10.1017/jfm.2018.66.

[47] M. S. Vázquez, O. Métais, Large-eddy simulation of the turbulent flow through a heated square duct, Journal of Fluid Mechanics 453 (2002) 201–238. doi:10.1017/S0022112001006887.

[48] H. Yang, T. Chen, Z. Zhu, Numerical study of forced turbulent heat convection in a straight square duct, International Journal of Heat and Mass Transfer 52 (13-14) (2009) 3128–3136. doi:10.1016/j.ijheatmasstransfer.2009.01.029.

[49] H. Zhang, F. X. Trias, A. Gorobets, Y. Tan, A. Oliva, Direct numerical simulation of a fully developed turbulent square duct flow up to Re τ = 1200, International Journal of Heat and Fluid Flow 54 (2015) 258–267. doi:10.1016/j.ijheatfluidflow.2015.06.003.

[50] W. H. Lowdermilk, W. F. Weiland, N. B. Livingood, Measurement of Heat-Transfer and Friction Coefficients for Flow of Air in Noncircular Ducts at High Surface Temperatures (1954).

[51] C. A. Sleicher, Jr., M. Tribus, Heat Transfer in a Pipe With Turbulent Flow and Arbitrary Wall-Temperature Distribution, Transactions of the American Society of Mechanical Engineers 79 (4) (1955) 789–797. doi:10.1115/1.4013150.

[52] N. A. Cumpsty, J. H. Horlock, Averaging Nonuniform Flow for a Purpose, Journal of Turbomachinery 128 (1) (2005) 120–129. doi:10.1115/1.2098807.

[53] R. Winterton, Where did the Dittus and Boelter equation come from?, International Journal of Heat and Mass Transfer 41 (4-5) (1998) 809–810. doi:10.1016/S0017-9310(97)00177-4.

[54] R. G. Deissler, W. F. Weiland, W. H. Lowdermilk, Analytical and experimental investigation of temperature recovery factors for fully developed flow of air in a tube (Sep. 1958).

[55] C. Hong, H. Katanoda, Y. Asako, M. Faghri, Temperature recovery factor for gaseous nitrogen flow in a microtube, International Journal of Heat and Mass Transfer 202 (2023) 123688. doi:10.1016/j.ijheatmasstransfer.2022.123688.

[56] G. Ackermann, Plattenthermometer in Strömung mit großer Geschwindigkeit und turbulenter Grenzschicht, Forschung auf dem Gebiet des Ingenieurwesens A 13 (6) (1942) 226–234. doi:10.1007/BF02585341.

[57] M. Ciofalo, J. Stasiek, M. W. Collins, Investigation of flow and heat transfer in corrugated passages—II. Numerical simulations, International Journal of Heat and Mass Transfer 39 (1) (1996) 165–192. doi:10.1016/S0017-9310(96)85014-9.

[58] M. Teitel, R. Antonia, Heat transfer in fully developed turbulent channel flow: Comparison between experiment and direct numerical simulations, International Journal of Heat and Mass Transfer 36 (6) (1993) 1701–1706. doi:10.1016/S0017-9310(05)80080-8.

[59] M. Rokni, T. B. Gatski, Predicting turbulent convective heat transfer in fully developed duct flows, International Journal of Heat and Fluid Flow 22 (4) (2001) 381–392. doi:10.1016/S0142-727X(01)00104-7.

[60] A. G. Ramgadia, A. K. Saha, Study of fully-developed turbulent flow and heat transfer in a rotating wavy-walled duct, International Journal of Heat and Mass Transfer 144 (2019) 118578. doi:10.1016/j.ijheatmasstransfer.2019.118578.

[61] J. Pallares, L. Davidson, Large-eddy simulations of turbulent heat transfer in stationary and rotating square ducts, Physics of Fluids 14 (8) (2002) 2804–2816. doi:10.1063/1.1489684.

Appendix A. Film Comparisons for Pipe Flows

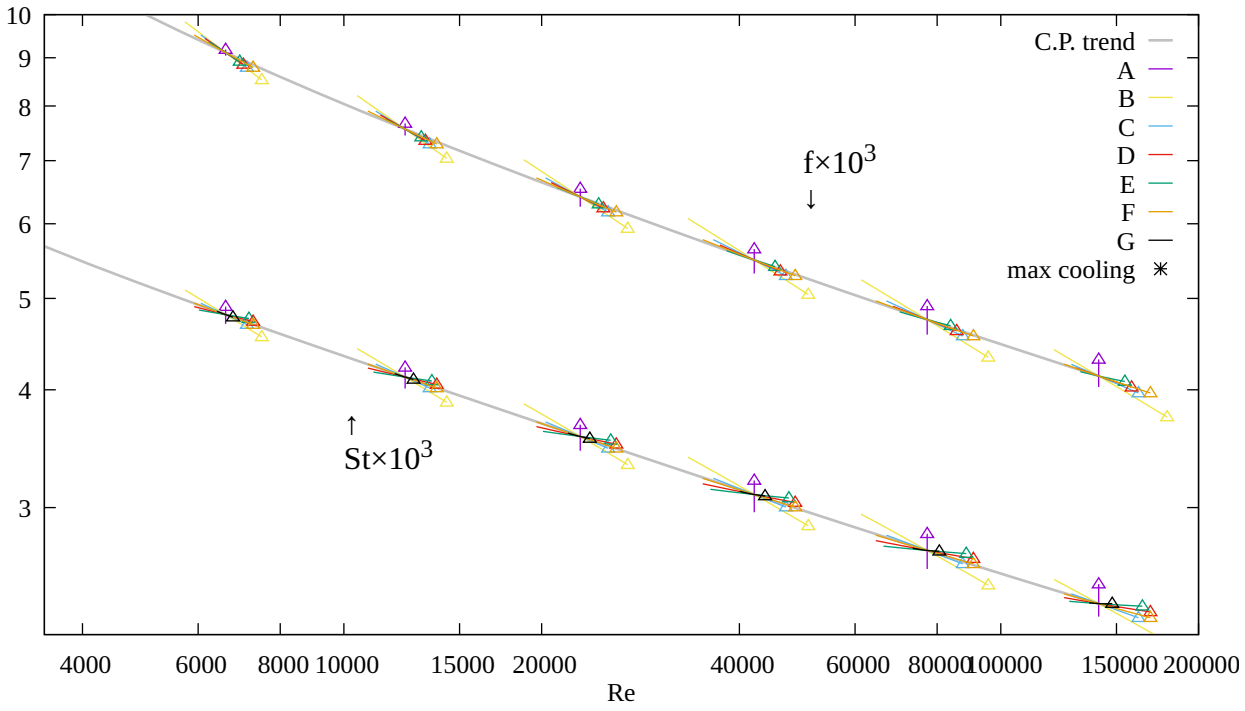

Figure A.23: *Re-f* & *Re-St* characteristics produced by varying heat flow to a pipe (H) at several fixed Re_b, see Table 3 for formulae

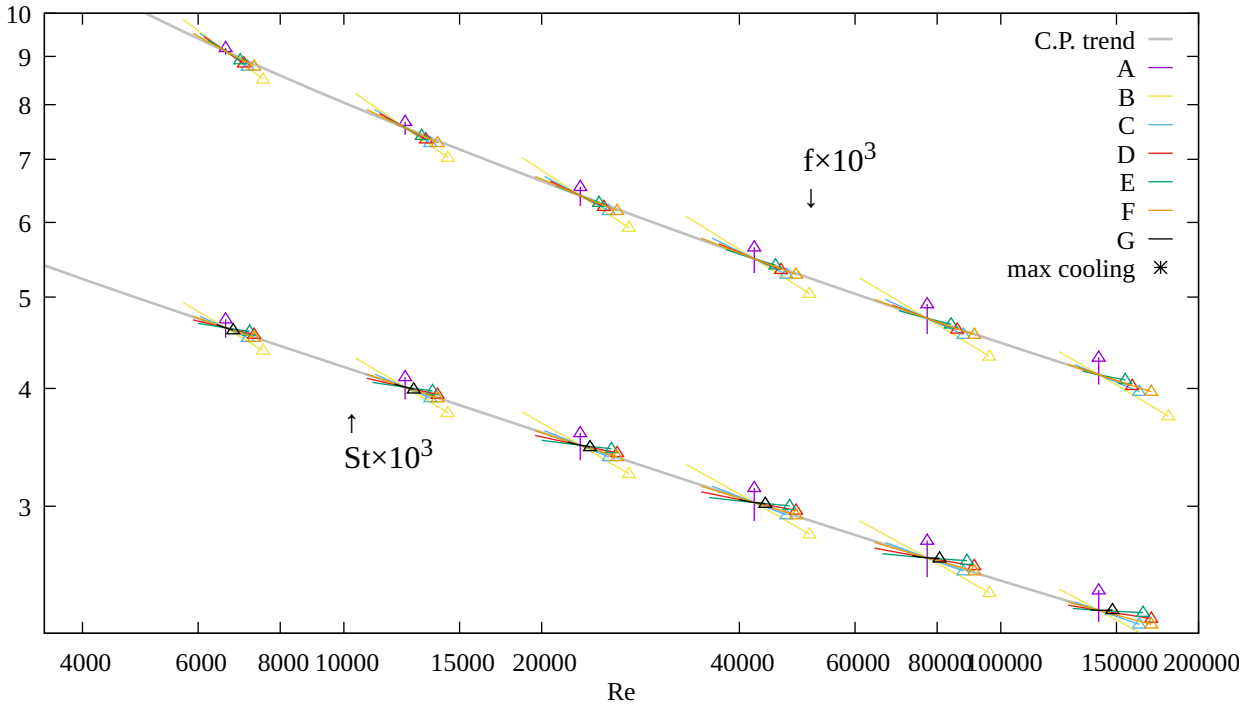

Figure A.24: *Re-f* & *Re-St* characteristics produced by varying heat flow to a pipe (T) at several fixed Re_b, see Table 3 for formulae